IPMSM Torque Control Strategies based on LUTs and VCT feedback for Robust Control under Machine Parameter Variations

E. Trancho[1], E. Ibarra[1], A. Arias[2], C. Salazar[1], I. Lopez[1], A. Diaz de Guereñu[1], A. Peña[1]
[1]Tecnalia Research and Innovation, Industry and Transport Unit
Parque Científico y Tecnológico de Bizkaia, c/ Geldo, Edif. 700, 48160 Derio (Spain)
[2]Institut d'Organització i Control, Universitat Politècnica de Catalunya.
Diagonal, 647, 08028 Barcelona
elena.trancho@tecnalia.com

***Abstract*—In recent years, Interior Permanent Magnet Synchronous Machines (IPMSMs) have attracted a considerable attention in the scientific community and industry for Electric and Hybrid Electric Vehicle (HEV) propulsion systems. Look-up Table (LUT) based Field Oriented Control (FOC) strategies are widely used for IPMSM torque control. However, LUTs strongly depend on machine parameters. Deviations of these parameters due to machine ageing, temperature or manufacturing inaccuracies can lead to control instabilities in the field weakening region. In this paper, two novel hybrid IPMSM control strategies combining the usage of LUTs and Voltage Constraint Tracking (VCT) feedbacks are proposed in order to overcome the aforementioned controllability issues. Simulation results that demonstrate the validity of the proposed approaches are presented.**

***Index Terms*—IPMSM, FOC, LUT, VCT**

I. Introduction

Nowadays, Interior Permanent Magnet Synchronous Machines (IPMSMs) are receiving a considerable attention in a number of high performance applications, such as Electric Vehicles (EVs) and Hybrid Electric Vehicles (HEVs) due to their high power density and high efficiency over wide speed and torque ranges [1]–[4].

A variety of torque control methods for IPMSMs can be found in the scientific literature [1], [5]–[15]. Look-up-Table (LUT) based Field Oriented Control (FOC) strategies (figure 1) are one of the most commonly used torque control techniques [6]–[8]. These techniques are relatively simple to implement and require low computational cost. However, the LUT approach has the following drawbacks:

- LUTs can require a relatively high amount of memory, depending on their size and number of dimensions.
- Machine electric parameters may vary due to manufacturing tolerances, machine ageing or temperature variations. Thus, the torque control may be affected by irregularities and unconsciousness during operation, leading to possible instabilities in the Field Weakening (FW) region.

Taking the latter into account, this paper presents a robust 2D-LUT based current control, ensuring controllability under electrical parameter variations and/or resolver offset determination errors. In order to achieve this goal, two novel Voltage-Constraint-Tracking (VCT) based feedback strategies are proposed to guarantee that the system remains under the maximum voltage constraint in the field weakening region. As far as the autors are concerned, hybrid solutions integrating both LUT-based control and voltage feedback have not been deeply studied in scientific literature.

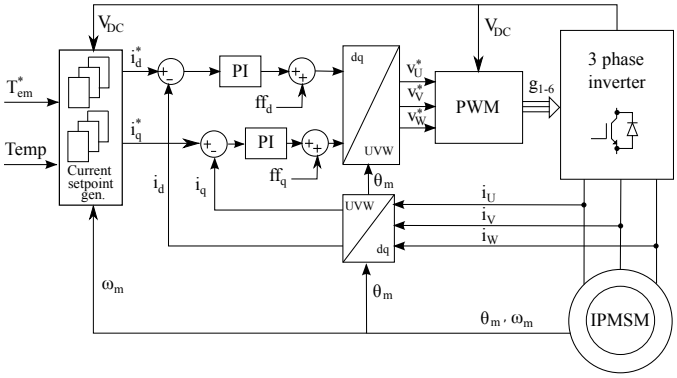

Fig. 1. General diagram of a 4D-LUT based IPMSM field oriented control.

II. LUT based FOC control

A. IPMSM control fundamentals

The stator voltages of an IPMSM in the dq synchronous rotating reference frame can be obtained as [16]:

$$v_d = R_s i_d + \frac{d\Psi_d}{dt} - \omega_e \Psi_q, \tag{1}$$

$$v_q = R_s i_q + \frac{d\Psi_q}{dt} + \omega_e \Psi_d, \tag{2}$$

where the magnetic fluxes are:

$$\Psi_d = L_d i_d + \Psi_{pm}, \tag{3}$$

$$\Psi_q = L_q i_q. \tag{4}$$

being v_d, v_q, i_d and i_q the stator voltages and currents; R_s, L_d and L_q the stator resistance and inductances, Ψ_{pm} the

magnetic flux of the permanent magnets and ω_e the electrical rotor frequency ($\omega_e = P\omega_{mech}$, being P the IPMSM pole-pair number). The electromagnetic torque produced by the IPMSM is obtained as:

$$T_{em} = \frac{3}{2}P\{\Psi_{pm}i_q + (L_d - L_q)i_d i_q\}. \quad (5)$$

In general, IPMSMs for EV and HEV applications are characterized by suffering high magnetic saturation [2], [17]; thus, $L_d = f_1(i_d, i_q)$ and $L_q = f_2(i_d, i_q)$. Temperature variations can also have a relevant influence [18], [19], reducing the flux produced by permanent magnets and leading to variations in the torque production. FOC is the most popular technique for torque control of synchronous machines [20]. Figure 1 shows the general 4-D LUT based FOC torque control diagram for an IPMSM. In this approach, the optimal current setpoints are determined from the operation conditions of the machine and data stored in two precalculated LUTs.

B. IPMSM torque control operation regions

IPMSM drives have speed and torque constraints, mainly due to inverter ratings and available DC link voltage limitations [21]. This constraints can be represented with the following mathematical expressions:

$$\sqrt{i_d^2 + i_q^2} \leq I_{max}, \quad (6)$$

$$L_d^2(i_d + \frac{\Psi_{pm}}{L_d})^2 + L_q^2 i_q^2 \leq (\frac{V_{max}}{w_e})^2, \quad (7)$$

where I_{max} and V_{max} are the maximum allowable stator current and voltage, respectively. The current limit curve (6) produces a circumference of radius I_{max} in the stator currents dq plane. Similarly, (7) produces ellipses whose radius decreases when the electrical machine speed increases (figure 2(a)). The IPMSM machine must be controlled such as the dq plane current vector lies simultaneously within the current constraint circumference and voltage constraint ellipse [21]. According to these constraints and considering an arbitrary torque inferior to the maximum one, four operation regions for the IPMSM can be distinguished (figures 2(a) and 2(b)) [5], [21], [22]:

I **Maximum Torque Per Ampere (MTPA) region.** An MTPA curve exists in the stator current dq reference frame which ensures a maximum torque per applied current modulus (figure 2(b), region I). Minimum ohmic losses are obtained if this curve is tracked.

II **Field weakening region without torque reduction.** In order to extend the speed operation region of an IPMSM, the control strategy consists of reducing the i_d current. In a given region, this is achieved without loosing torque capability, as i_q^* can be recalculated to maintain the reference torque (figure 2(b), region II). This region can be extended until the speed w_b is reached (figure 2(a)), where the speed and current limit curves intersect with each other.

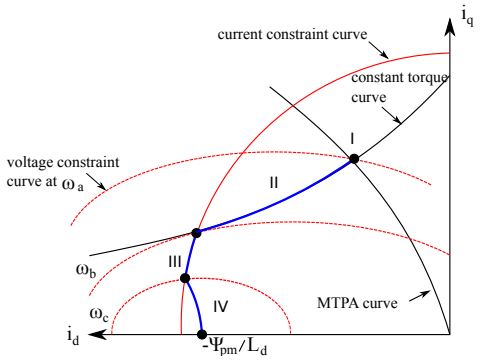

(a) Optimal trajectory of the stator currents in the dq plane taking into account the current and voltage constraints.

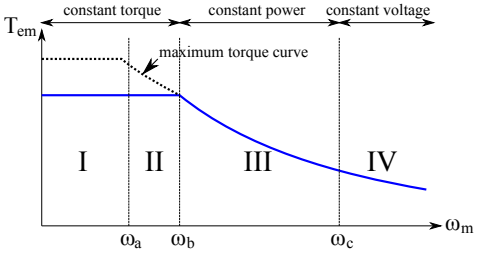

(b) IPMSM optimum operation regions for an arbitrary torque $T_{em} < T_{em}^{max}$: MTPA (I), field weakening (I), field weakening with torque reduction (III) and MTPV (IV).

Fig. 2. IPMSM optimal control trajectories and regions.

III **Field weakening region with torque reduction.** When current constraint circumference is reached, the torque capability is reduced in field weakening operation (figure 2(b), region III). In order to achieve maximum torque in this region, the current set point vector must be positioned in the intersection between the voltage and current constraint curves.

IV **Deep field weakening region.** In this operation region, also known as Maximum Torque Per Voltage (MTPV) region, the torque production capability is maximized for a constant stator voltage value (figure 2(b), operation region IV). The MTPV region only exists for a given IPMSM if $\Psi_{pm}/L_d \leq I_{max}$ condition is fulfilled, and can be mathematically determined [5].

C. LUT dimensioning

The dimensions required by current set-point generation LUTs can depend on the specific electric machine and application (for example, whether DC-link voltage varies or not), and also on the required torque production precision (rotor temperature dependency). As an example, figure 1 shows a 4D-LUT approach which requires rotor temperature knowledge. This temperature can be obtained using telemetry systems, infrared sensors, etc. [18], [19], avoiding the use of cables, or can be estimated from back EMF observers [18], [19]. However, at low and zero speeds, such observers tend to fail due to the lack of back Electro-Motive Force (back-EMF).

Thus, it is complicated to achieve a good rotor temperature estimation in the whole motor operation range.

Due to the complexity and/or additional cost of the aforementioned solutions, these are not of common practice in industrial applications [19]. Generally, the deviations produced by temperature effects are accepted and no compensation action is performed. On the other hand, the LUT dimension related to DC-link voltage variations can be eliminated using the speed normalization concept [13]. From (7), the maximum stator voltage can be derived as:

$$V_{max} = \omega_e \sqrt{(L_d i_d + \Psi_{pm})^2 + (L_q i_q)^2}. \tag{8}$$

In a two-level three-phase Voltage Source Inverter (VSI) fed machine, the maximum achievable phase voltage for the linear modulation region (when Space Vector modulation or PWM with third harmonic injection is adopted) is:

$$V_{max} = \frac{V_{DC}}{\sqrt{3}}. \tag{9}$$

A normalized voltage (V_{DC}^{norm}), which can be the minimum or the nominal DC-link voltage value, can be selected to define the μ normalization coefficient [13]:

$$\mu = \frac{V_{DC}}{V_{DC}^{norm}}. \tag{10}$$

Substituting (10) into (9), the following expression is obtained:

$$V_{max} = \frac{V_{DC}}{\sqrt{3}} = \frac{\mu V_{DC}^{norm}}{\sqrt{3}} = \mu V_{max}^{norm}, \tag{11}$$

while substituting (11) into (8), the following speed normalization equation is obtained:

$$\omega_e = \frac{\mu V_{max}^{norm}}{\sqrt{(L_d i_d + \Psi_{pm})^2 + (L_q i_q)^2}} = \mu \omega_e^{norm}. \tag{12}$$

When DC-link voltage increases, ω_e^{norm} becomes smaller than the real electrical speed ω_e. This is equivalent to a displacement of the speed vs torque curve towards the right side (figure 3), expanding the voltage limit. The opposite occurs when the DC-link voltage decreases. Thus, the normalized speed can be calculated and used as an input for a 2-D LUT calculated for the normalization DC-link voltage (V_{DC}^{norm}) operation conditions.

Advantages of this approach become clear, because the amount of memory resources needed for algorithm implementation in a microprocessors is highly reduced.

III. Proposed VCT Feedback Strategies for Robust IPMSM Control under Machine Parameter Variations

A. Introduction

In LUT based control schemes, parameter deviations can produce instabilities in the field weakening and MTPV regions, as the current trajectories stored in such LUTs depend on

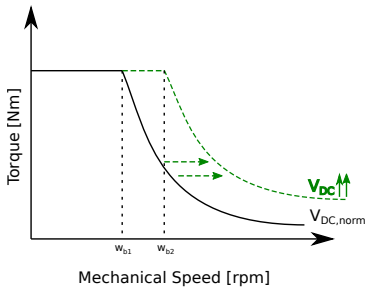

Fig. 3. Torque and Speed curve in DC-link voltage variation.

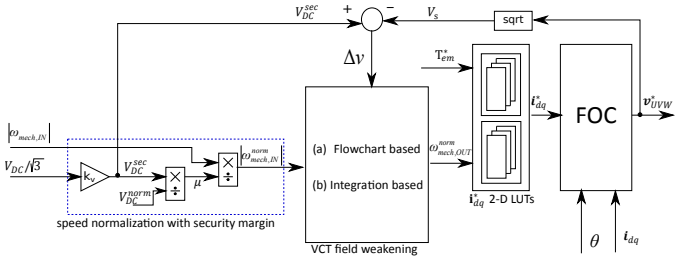

Fig. 4. LUT based current reference determination using the speed normalization concept and proposed VCT feedback strategies.

a given set of electric machine parameters. For that reason, it is of interest to include an online field weakening control loop to counteract these parameter uncertainties. If the electric machine contains an MTPV region, both i_d and i_q set-points should be simultaneously controlled by the online feedback loop. Traditional field weakening strategies only rely on the modification of i_d [13]. However, both i_d and i_q can be simultaneously controlled by regulating the parameter μ or the normalized mechanical speed $\omega_{mech}^{norm} = \omega_e^{norm}/P$ (figure 4).

The proposed control strategies are composed of two main blocks (figure 4):

- **Speed normalization block, including security margin:** From the normalized speed described in section II-C an additional security margin is applied multiplying the measured $V_{DC}/\sqrt{3}$ by a parameter k_v (in per unit). k_v is chosen to ensure that the voltage limit is never reached. Overmodulation is possible adjusting $k_v > 1$. However, overmodulation is avoided in this particular application, forcing $k_v < 1$.
- **VCT Field weakening block:** The normalized speed is controlled according to the actual value of the stator voltage (V_s) and the DC-link voltage multiplied by the security margin k_v. Instead of using a PI controller, whose gain adjustment is not straightforward, two VCT solutions have been adopted:
  (a) Flowchart based normalized speed control.
  (b) Integration based normalized speed control.

The proposed VCT strategies aim to maintain the operating point close to the voltage limit in both FW and MTPV regions. To ensure the latter, a parameter defining the VCT voltage

error, Δv, is included in both methods:

$$\Delta v = \frac{V_{DC} k_v}{\sqrt{3}} - V_s, \tag{13}$$

where V_s is the actual value of the stator voltage, commanded by the inverter.

The advantage of these methods is that no machine parameters are needed in their calculations. In the following, both proposed VCT alternatives are described in detail.

B. Flowchart based normalized speed control

The proposed strategy follows the flowchart shown in figure 5. This strategy is based on the solution proposed in [12]. At the beginning, the flowchart checks whether V_s is higher or lower than the voltage limit, i.e., flowchart checks the sign of Δv. If $\Delta v < 0$, variable $status$ is set to 0 to indicate that VCT strategy should be activated. In normal operation region ($status = 1$), no VCT strategy is activated; thus the output speed remains invariable. As for the FW process ($status = 0$), the flowchart is divided in two branches, by checking again the sign of Δv. If the voltage vector is not saturated, "A" branch will be selected. Otherwise, "B" branch will be activated.

When selecting "A" branch, VCT operation is activated and the inverter's output voltage is saturated, reaching the voltage limit. In "A", the normalized speed needs to be increased:

$$|\omega^{norm}_{mech,OUT}(k)| = |\omega^{norm}_{mech,OUT}(k-1)| + |\Delta v| * \alpha, \tag{14}$$

where α is a positive parameter. On the other hand, when "B" branch is activated, the normalized speed should be reduced:

$$|\omega^{norm}_{mech,OUT}(k)| = |\omega^{norm}_{mech,OUT}(k-1)| - |\Delta v| * \beta, \tag{15}$$

being β is a positive parameter.

Both α and β parameters should be manually adjusted for each particular application. The decision of whether VCT strategy needs to continue activated or not is processed in "B" branch. If the calculated normalized speed $|\omega^{norm}_{mech,OUT}(k)|$ is smaller than the reference normalized speed $|\omega^{norm}_{mech,IN}(k)|$, the flowchart assumes that VCT operation should be stopped. Therefore, $status$ signal is set to 1 and the flowchart re-starts its algorithm, analysing the polarity of Δv.

In summary, the proposed algorithm decides whether modify or keep the commanded normalized speed. When the field weakening is activated, branch "A" and "B" modify the commanded normalized speed, in order to maintain the voltage vector in the DC-link voltage limit.

C. Integration based normalized speed control

In figure 6 a diagram of the proposed integration based VCT feedback is shown. This strategy also aims to correct the commanded normalized speed, ensuring that inverter output voltage remains under the voltage limit in both FW and the MTPV regions.

The integration based voltage closed loop algorithm can be defined as:

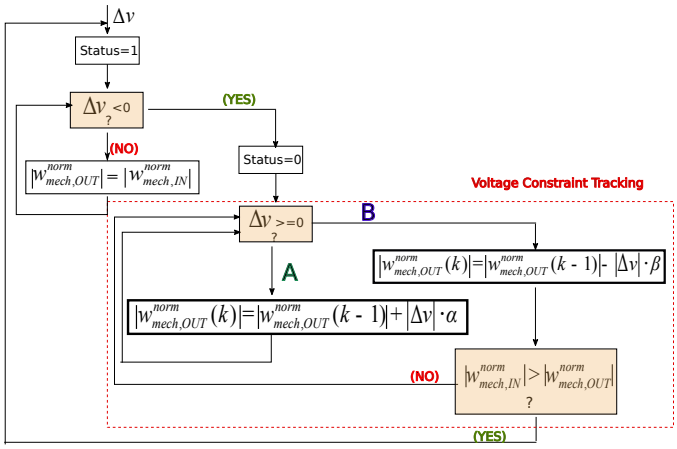

Fig. 5. Flowchart of VCT for normalized speed command generation.

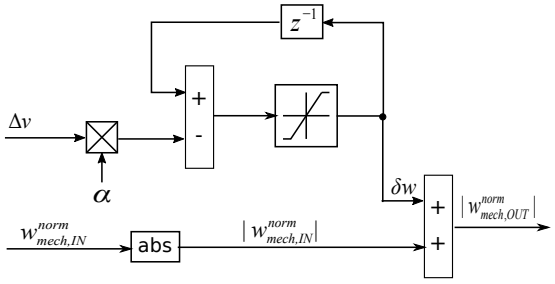

Fig. 6. Integration based normalized speed control for Voltage Constraint Tracking based field weakening.

$$|\omega^{norm}_{mech,OUT}(k)| = |\omega^{norm}_{mech,IN}(k)| + \delta\omega(k), \tag{16}$$

where

$$\delta\omega(k) = \delta\omega(k-1) - \alpha\Delta v, \tag{17}$$

being α a positive constant and

$$\delta\omega(k) = \begin{cases} 0 & if\ \delta\omega(k) \leq 0, \\ \delta\omega(k) & if\ 0 < \delta\omega(k) \leq \delta\omega_{max}, \\ \delta\omega_{max} & if\ \delta\omega(k) > \delta\omega_{max} \end{cases} \tag{18}$$

As expressed in (16), this strategy modifies the normalized speed to be introduced in the 2D LUT correcting its magnitude throughout $\delta\omega(k)$ term.

When the inverter output voltage is not saturated ($\Delta v \geq 0$), the normalized speed corrector term $\delta\omega(k)$ tends to be negative. However, due to the saturation effect defined in (18), $\delta\omega(k)$ is limited only to positive values and thus this corrector doesn't modify the magnitude of $|\omega^{norm}_{mech,OUT}(k)|$. Therefore, when no voltage limit is reached, the speed output remains invariable. If the inverter output voltage exceeds the voltage limit ($\Delta v < 0$), the normalized speed needs to be increased in order to restore the stator voltage inside the voltage limit and avoid control instability. In this situation, the speed corrector $\delta\omega(k)$ tends to become positive, due to Δv polarity. Modifying the speed normalized magnitude, the stator voltage remains in

TABLE I
MOST SIGNIFICANT PARAMETERS OF THE SIMULATED IPMSM MACHINE.

Parameter	Symbol	Value	Units
Maximum power	P_N	100	kW
Maximum speed	w_{max}	3500	rpm
Stator Resistance	R_s	0.04	Ω
d-axis nominal inductance	L_d	1e−3	H
q-axis nominal inductance	L_q	1.7e−3	H
Permanent Magnet Flux linkage	Ψ_{PM}	0.178	Wb

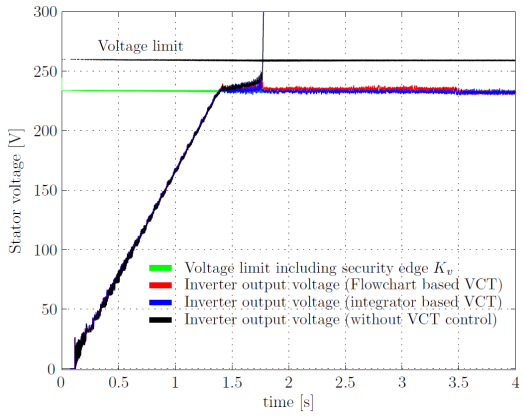

(a) VCT voltage control results of the proposed hybrid control strategies.

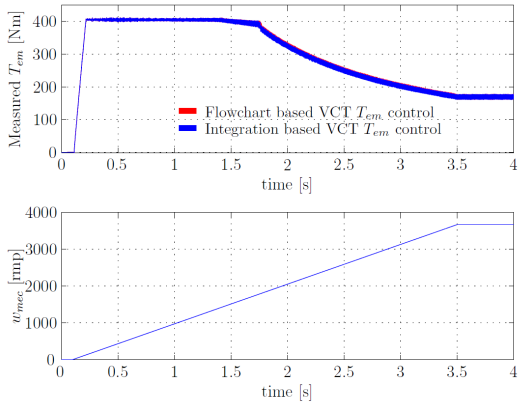

(b) VCT torque control results of the proposed hybrid control strategies.

Fig. 7. Proposed hybrid IPMSM control strategies simulation results.

the voltage limit curve, ensuring the voltage constraint tracking control loop.

The integration based speed control strategy only requires one parameter to be adjusted, instead of the couple of parameters α, β needed for the flowchart based algorithm.

IV. SIMULATION RESULTS

In order to validate the proposed control strategies, a 100 KW automotive IPMSM drive including magnetic saturation has been simulated in Matlab/Simulink environment. The FOC algorithm is executed every $90\mu s$, while the VCT together with the LUTs are executed at a higher sample-time ($2.5ms$), for integration optimisation issues. Variable DQ

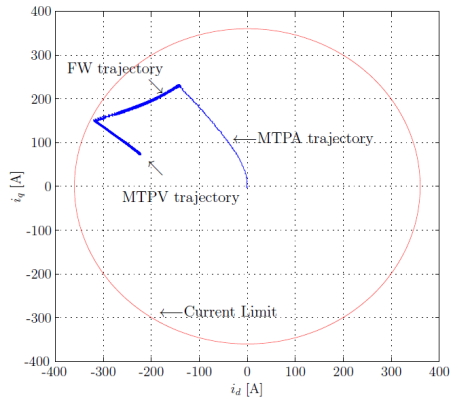

Fig. 8. dq plane currents trajectories and their correspondence to an operation mode.

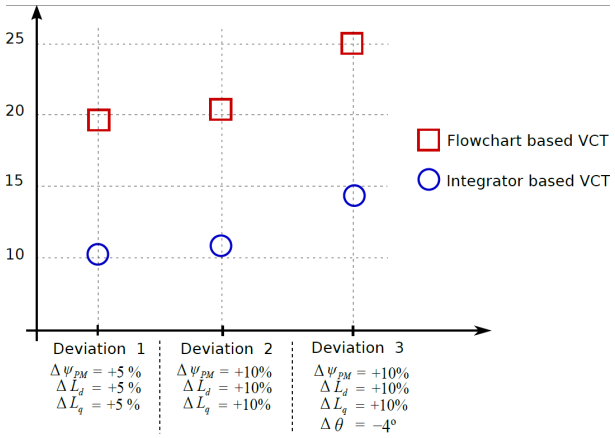

Fig. 9. VCT based alternatives comparison using ISE performance index.

(VDQ) approach [23] has been followed for IPMSM modelling and LUTs have been calculated based on the IPMSM magnetic model. The PI controllers have been tuned taking into account the delays introduced by the digital control. Table I shows the most significant parameters of the simulated IPMSM. This machine presents the typical saturation profiles of a medium-power IPMSM automotive propulsion electric machine. As the influence of the magnetic saturation in the d-axis cannot be decoupled between the permanent magnet flux linkage (ψ_{pm}) and the stator flux (ψ_d), ψ_{pm} is considered constant, while magnetic saturation is entirely represented in the d-axis inductance. To validate the controllability using the proposed VCT strategies, the following parameters deviation have been set: $\delta\Psi_{pm} = +10\%$, $\delta L_d = +10\%$.

Figure 7(a) shows the results of the different control approaches of conventional FOC control including the 2D-LUT current set point generation with and without a VCT control. It can be seen that when VCT control is not active in the loop, the voltage limit is exceeded and the system becomes unstable due to the electrical parameter variations. However, an effective VCT control is achieved when using both proposed strategies (figure 7(a)). Currents trajectory in the dq plane and their

correspondance to the different operation modes are shown in figure 8. A proper torque control is achieved despite the introduced parameter variation (figure 7(b)). In order to analyse and compare the system's performance using the proposed strategies, performance indices have been adopted [24], being the system optimum when the index reaches a minimum value. The performance index used is the Integral of the Square of the Error (ISE), defined as:

$$ISE = \int_0^T e^2(t)dt. \tag{19}$$

Figure 9 shows the results obtained using both flowchart and integrator based VCT control techniques, assuming different parameter deviations. In the three different conditions tested, integrator based VCT technique minimizes the ISE index.

V. Conclusions

As it has been demonstrated in simulation, current trajectories stored in such LUT depend of electric parameters, thus uncontrollability may be produced when parameter variations occur due to machine ageing or temperature variation, among other factors). The proposed flowchart based and integrator based voltage constraint tracking solutions ensure robust control in the whole operation range, being activated only when voltage constraint limit is reached. The advantage of the aforementioned strategies is that no machine parameters are needed in their calculations. While the flowchart based method implementation requires two parameters to set, only one parameter to be adjusted is needed in the integration based one. In both cases, simulation results of these approaches verify the smooth tracking of the voltage limit when required, keeping the voltage constraint tracking error within an acceptable range.

For future work, further experimental results will be carried out on IPMSM used on an EV prototype.

Acknowledgment

The present work is partially supported by the Basque Goverment under the projects KT4eTRANS (ELKARTEK program KK-2015/00047), FPGAmc (EMAITEK program) and by the spanish projects DPI2013-41224-P (Ministerio de Educación) and 2014 SGR 267 (AGAUR).

References

[1] B. Asaei and B. Rahrovi, "Minimum-copper-loss control over full speed range of an ipmsm drive for hybrid electric vehicle application," in *IEEE Vehicle Power and Propulsion Conference (VPPC)*, 2010.

[2] J. Cintron-Rivera, S. Foster, C. Nino-Baron, and S. E.G., "High performance controllers for interior permanent magnet synchronous machines using look-up tables and curve-fitting methods," in *IEEE International Electric Machines & Drives Conference (IEMDC)*, 2013, pp. 268–275.

[3] T. Finken, M. Hombitzer, and K. Hameyer, "Study and comparison of several permanent-magnet excited rotor types regarding their applicability in electric vehicles," in *Emobility - Electrical Power Train Conference*, 2010.

[4] M. Hinkkanen, Z. Qu, H. Awan, A. A., T. Tuovinen, and F. Briz, "Current control for ipmsm drives: Direct discrete-time pole-placement design," in *Proc. of the IEEE Workshop on Electrical Machines Design, Control and Diagnosis (WEMDCD)*, 2015.

[5] S. Jung, J. Hong, and K. Nam, "Current minimizing torque control of the ipmsm using ferrari's method," *IEEE Transactions on Power Electronics*, pp. 5603–5617, 2013.

[6] M. Meyer and J. Bocker, "Optimum control for interior permanent magnet synchronous motors (ipmsm) in constant torque and flux weakening range," in *EPE-PEMC Conference*, 2006, pp. 282–286.

[7] G. Rang, J. Lim, K. Nam, H. Ihm, and H. Kim, "A mtpa control scheme for an ipm synchronous motor considering magnet flux variation caused by temperature," in *Applied Power Electronics Conference and Exposition (APEC)*, 2004.

[8] Y. Kim and S. Sul, "Torque control strategy of an ipmsm considering the flux variation of the permanent magnet," in *Industry Applications Conference*, 2007.

[9] J. Cintron-Rivera, S. Foster, W. Zanardelli, and E. Strangas, "High performance controllers based on real parameters to account for parameter variations due to iron saturation," in *NDIA Ground Vehicle Systems Engineering and Technology Symposium*, 2013.

[10] T. Herold, D. Franck, E. Lange, and K. Hameyer, "Extension of a d-q model of a permanent magnet excited synchronous machine by including saturation, cross-coupling and slotting effects," in *International Electric Machines and Drives Conference*, 2011.

[11] S. K. S. J.M, Kim, "Speed control of interior permanent magnet synchronous motor drive for the flux weakening operation," *IEEE TRANSACTIONS ON INDUSTRY APPLICATIONS*, vol. 33, no. 1, pp. 43 – 48, January 1997.

[12] S. Shue and C. Pan, "Voltage-constraint-tracking-based field-weakening control of ipm synchronous motor drives," *IEEE Transactions on Industrial Electronics*, vol. 55, no. 1, pp. 340–347, 2008.

[13] J. Lee, C. Won, B. Lee, J. Baek, K. Han, and U. Chung, "Ipmsm torque control method considering dc-link voltage variation and friction torque for ev/hev applications," in *Proc. of the IEEE Vehicle Power and Propulsion Conference*, 2012, pp. 1063–1069.

[14] V. Nguyen, B.H and. Han and M. C.T., "High performance current control of ipmsm for electric vehicles drives using disturbance observer," in *In proc. of the Vehicle IEEE Power and Propulsion Conference (VPPC)*, 2015.

[15] C. et al., "Feedback linearization direct torque control with reduced torque and flux ripples for ipmsm drives," *IEEE Transactions on Power Electronics*, vol. 31, no. 5, pp. 3728–3737, 2015.

[16] P. Seibt and A. Fischer, *Description of the Cross Saturation in an IPMSM for Electric Vehicles Using Bicubic Splines*, ser. Analysis and Simulation of Electrical and Computer Systems, Lecture Notes in Electrical Engineering. Springer, 2015, vol. 324.

[17] W. Peters, O. Wallsccheid, and J. Bockere, "A precise open-loop torque control for an interior permanent magnet synchronous motor (ipmsm) considering iron losses," in *Annual Conference of the IEEE Industrial Electronics Society (IECON)*, 2012, pp. 2877–2882.

[18] A. Specht and J. Bocker, "Observer for the rotor temperature of ipmsm," in *Proc. of the International Power Electronics and Motion Control Conference (EPE-PEMC)*, 2010.

[19] M. Ganchev, C. Kral, and T. Wolbank, "Sensorless rotor temperature estimation of permanent magnet synchronous motor under load conditions," in *Proc. of the IEEE Industrial Electronics Conference (IECON)*, 2012, pp. 1989–1994.

[20] X. Garcia, B. Zigmund, A. Terlizzi, T. Pavlanin, and L. Salvatore, "Comparison between foc and dtc strategies for permanent magnet synchronous motors," *Advances in Electrical and Electronic Engineering*, pp. 76–81, 2004.

[21] S. Morimoto, Y. Takeda, T. Hirasa, and K. Taniguchi, "Expansion of operating limits for permanent magnet morot by current vector control considering inverter capacity," *IEEE Transactions on Industry Applications*, vol. 26, no. 5, pp. 866–871, 1990.

[22] C. Pan and S. Sue, "A linear maximum torque per ampere control for ipmsm drives over full-speed range," *IEEE Transactions on Energy Conversion*, vol. 20, no. 2, pp. 359–366, 2005.

[23] C. Dufour, S. Cense, T. Yamada, R. Imamura, and J. Belanger, "Fpga permanent magnet synchronous motor floating-point models with variable-dq and spatial harmonic finite-element analysis solvers," in *International Power Electronics and Motion Control Conference, EPE-PEMC ECCE Europe*, vol. LS6b.2, 2012, pp. 1–10.

[24] Dorf and Bishop, *Modern Control Systems*. Pearson/Prentice-Hall, 2005.